Sensors and Actuators A 167 (2011) 502–511

Contents lists available at ScienceDirect

Sensors and Actuators A: Physical

journal homepage: www.elsevier.com/locate/sna

Development and characterization of a packaged mechanically actuated microtweezer system

Brock A. Wester[a,b,c,d,*], Swaminathan Rajaraman[d], James D. Ross[d], Michelle C. LaPlaca[a,c], Mark G. Allen[b,d]

[a] Laboratory for Neuroengineering, Georgia Institute of Technology, United States
[b] Microelectronics Research Center, Georgia Institute of Technology, United States
[c] Emory University School of Medicine, United States
[d] NanoGrip Technologies, Inc., United States

ARTICLE INFO

Article history:
Received 25 September 2010
Received in revised form
22 December 2010
Accepted 7 January 2011
Available online 5 March 2011

Keywords:
MEMS
Microtweezers
Packaging
Micromanipulation
Biological interfacing
Mechanical actuation

ABSTRACT

This paper presents the successful design, modeling, fabrication, packaging, and characterization of a mechanically actuated micro-electro-mechanical-systems (MEMS) microtweezer. This complete and modular MEMS system has minimal manufacturing complexity and can be augmented to any standard micromanipulator or positioning system. The microtweezer is mechanically actuated and hence has minimal impact on the surrounding microenvironment, a key consideration for micromanipulation. The microtweezer components are fabricated utilizing standard electroplating based processes. The microtweezer is functionally attached to a tether-cable system packaged within a stainless steel luer needle, which can be mounted to a manual controller with a luer interface. The controller, which provides axial rotational movement of the microtweezer, can be attached to any positioning stage to allow 5+ degrees of movement freedom. Mechanical modeling and characterization of the system shows that precise and controlled tool actuation is achieved with tip closing forces averaging 360 mN over an actuation range of 125 μm. The system's performance and ease of use can provide the means to create and enhance a multitude of experimental preparations previously not possible.

1. Introduction

To allow for experimentation and interfacing with a variety of material, chemical, and biological microenvironments, there have been a number of platform based (microelectrode arrays, lab-on-a-chip devices, platform microfluidics and sensors) and non-platform based (insertable-shank electrodes, microgrippers, microtweezers) micro-electro-mechanical system (MEMS) devices created [1–3]. While platform MEMS devices allow for a multitude of interfacing applications, the ability to manipulate or position microstructures is limited, as are the degrees of movement freedom. However, microtweezers and similar microtools offer an attractive option to meet the increasing need to simultaneously interface with and manipulate micro-sized objects such as microfabricated and material constructs, optical fibers and crystals, cells and tissues, fluorescent and positional markers, and biological structures.

Independent of application, one of the most critical aspects to MEMS device design and efficacy is developing an interfacing mechanism, or package, that provides important application-dependent functionalities, such as physical and environmental protection, translation of mechanical movement, fluid transfer, or electrical connectivity [4]. Implementation of this packaging is especially important for non-platform systems due to intended or unintended movement, which can complicate the design and reduce stability in functional and physical connectivity. Packaging considerations in MEMS, semiconductors, and biomedical devices is critical and can account for over 70% of the cost and time development of the final device [5].

The packaging system presented in this paper utilizes a modular, segmented mechanical mechanism, and allows previously developed MEMS microtweezers [6,7] to be used in a variety of environments and applications. As the tool presented here provides acuity of control, repeatability, and miniaturization, it can also play a more direct role in experimentation, such as isolating material and tissue samples for chemical and mechanical characterization and manipulation. Microtweezers tailored to these applications can allow for a significant variety of experimental preparations previously not thought possible. In addition to benefiting MEMS interfacing and assembly, microstructure positioning and manipulation, and biomedical research, these devices could be adapted to support remote, minimally invasive surgi-

* Corresponding author at: Laboratory for Neuroengineering, Georgia Institute of Technology, 313 Ferst Drive, Atlanta, GA 30332, United States. Tel.: +1 404 944 3795.
E-mail address: brock@gatech.edu (B.A. Wester).

0924-4247/$ – see front matter © 2011 Elsevier B.V. All rights reserved.
doi:10.1016/j.sna.2011.01.005

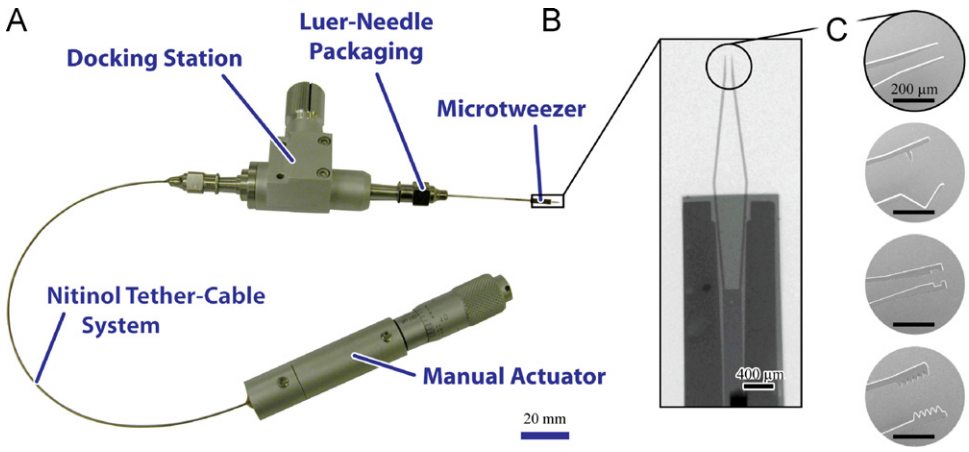

Fig. 1. (A) Photo of the current microtweezer packaging and manual controller system. The microtweezer is mechanically packaged with a stainless steel luer needle. The manual mechanical controller consists of a docking station, a manual linear actuator with a micrometer knob, and a nitinol tether-cable system to physically and functionally connect them. (B) X-ray of assembled microtweezer. (C) SEM images of various tweezer tips.

cal and dissection procedures, both in a clinical and experimental setting.

For devices that actively and mechanically interface with microenvironments for the purpose of micromanipulation, electrical, thermal, piezoelectric, laser, or shape memory alloy based actuation mechanisms have been historically utilized due to established actuation techniques and microfabrication strategies [8–17]. However the use of these mechanisms have several limitations: (1) material limitations due to the required use of silicon-based microfabrication techniques to achieve electrically induced actuation, (2) mechanical and electrical variation from device to device due to inherent limitation in the actuation mechanism (i.e. the tuning of a piezo or electro-thermal driving signal for an actuator) [18], (3) modular construction of the microdevice and the electrical packaging can be expensive and unreliable, (4) interference from the microenvironment can alter or inhibit device performance (i.e. aqueous environment, heated systems, etc.), (5) limited actuation range or resolution, and (6) most importantly, these electrical, optical and thermal devices can dissipate heat into the local environment, as well as generate unintended and potentially damaging electrostatic fields and currents that limit the device's applications, especially when introduced into a biological environment.

The microtweezers reported in this paper employ a proprietary [19] micro-mechanical actuation mechanism based on position, precluding the need for thermal, optical or electrically sensitive materials, or for complex controllers. Tool tips are opened and closed due to their position within a sleeve, or box, and the relative motion of these two components can be delivered through a single axis direct-drive system. This actuation method is similar to other microtools [20], but our microtweezers: (1) have isolation of axial rotation and vertical translation; (2) benefit from microfabrication processes that allow the patterning of smaller features at the tweezer tips; and (3) modular fabrication allows for the potential to integrate friction-removing coatings [21,22].

This system consists of a luer based tool packaging and docking station, which allows plug-n-play docking of various microtools as well as rotation along the microtool axis. Remote actuation is achieved utilizing an actuator, or micrometer/motor attached to a tether-cable system. Because such a mechanism can be controlled either by a knob or motor, it could benefit from both the inherent tactile precision of a human user, or the automation of a computerized controller. These components can augment any standard micropositioner, allowing positioning in three-plus dimensions, plus the tool actuation and rotation. Given the simplicity of design and manufacturing requirements, these potentially disposable tools address needs in a variety of bio-medical, clinical, and experimental markets.

2. Device design and integration

2.1. MEMs microtweezer system

The microtweezer system is composed of four main components, (1) a packaged microtweezer tool, (2) a docking station, (3) a mechanical linear actuator, and (4) a positioning stage (Fig. 1). The microtool is a microfabricated MEMS microtweezer structure that is attached to a luer needle. Inside the housing of the luer needle is a spring loaded button that is functionally and physically connected to the microfabricated MEMS structure. This luer needle based packaging allows for mounting onto the docking station, which has a male luer fitting. The docking station provides rotational functionality of the microtool about the luer needle axis, as well as mounting of the system onto a stage using a custom mounting bracket. A linear actuator drives a spring-loaded rod through the docking station to drive the spring loaded button of the microtool package, which actuates the microtweezer. This linear actuator can be a manually driven micrometer head, stepper motor system, or any other motor actuator system. Such a system design allows for modularity and the ability to augment the microtool system to a variety of manual and automated positioning stages.

2.2. MEMS microtweezer design

Our previous work demonstrated the successful fabrication of a prototype microtweezer, which consisted of two main components: (1) a tool body that contains the tool beams and tips, and (2) a sleeve, or box that houses the tool body in an inner constrictive channel that physically engages the tool beams to close the tips (Fig. 2) [6,7]. Thus, these microtweezers use externally applied linear mechanical motion to achieve high-resolution tip control as the tool tips are opened and closed due to their position within the moving box. As the box moves forward, it also provides additional self-alignment of the tips, which is achieved by exerting equal forces from each side of the channel, and by the channel constricting vertical movement of the tweezer beams.

The box channel contains multiple segments of varying inner geometries as shown in Fig. 2: a regular drive section, and an overdrive section which provides additional actuation range to allow tool tips with larger separations between them to close completely, as well as multiple closing regimens with differing speeds. This sec-

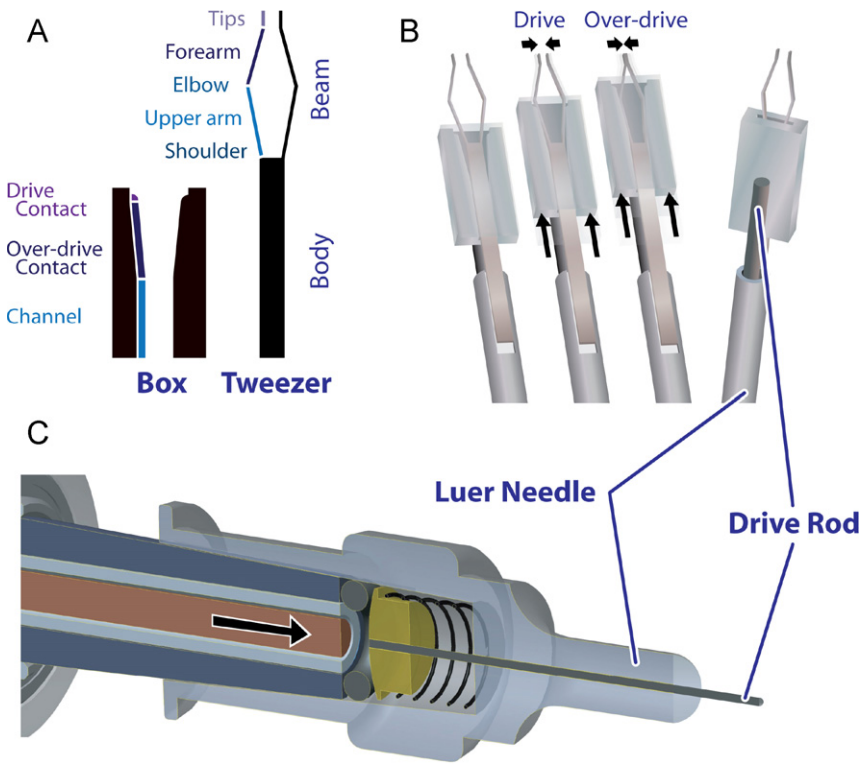

Fig. 2. (A) Schematic of MEMS box and tweezer showing key features, (B) box and tool tips actuation with arrow size demonstrating a 3:1 actuation ratio (linear box movement to tip closing), and (C) mechanical luer-needle packaging of microtweezer with needle and drive rod. The drive shaft (red) meets a rounded interface on the outside of the button resulting in a point contact, which limits torsional loading on the drive rod during axial rotation of the microtweezer.

tion additionally allows for increasing the force of closure to allow manipulation of heavier samples. The 2D patterned inner-channel geometries are relatively unconstrained, allowing a range of closing schemes to be employed for instrument customization, such as fast closing of bulk microtweezer tip separation, and then slow closing of the remaining tip separation prior to tip contact. Geometric tuning of the beams and channel leads to a distinct advantage in device design: a box movement of 1 μm translates into 300 nm of tip closure, providing a mechanical advantage, or 3:1 actuation resolution ratio. This tunable advantage lends itself to achieving high resolution tip movement in the submicron-scale.

The microtweezer body, tips, and box were originally microfabricated together in the same sample to eliminate the need for post-processing assembly, to limit opportunity for tool damage during assembly, and to ensure body and box alignment [6]. In the current manufacturing process, the box and tool body/tips are fabricated separately. Separate construction reduces the complexity of each fabrication process, allows direct process refinement, enables addition of finer features (e.g. over-drive section), and increases yield. While assembly of the two parts is required, the use of machined jigs that align the parts facilitates the directed insertion of the tweezer into the box and multiple insertions in parallel can be performed with the machined jigs increasing throughput. Fabricating the two components separately also allows for a more versatile selection of materials for the box and body (e.g. silicon boxes and metal microtweezers), tool tip geometries, and separate post-fabrication processing for tip sharpening, patterning and surface treatments (to allow for potential elimination of material incompatibilities). This modular design also creates a platform that permits future integration of various sensors on the tool tips, such as surface microelectrodes, position sensors, and strain gauges.

The selection of materials is important not only for the mechanical and material properties, such as tensile strength, elastic modulus, and surface attraction, but also for biological compatibility. The microtool body fabricated in this work has tips that are 40 μm wide and 20 μm thick. The body and box channel widths are 300 μm and 330 μm, respectively.

2.3. MEMS packaging design

The mechanical microtool packaging consists of a physical luer interface between the microtool and the docking station, and includes an internal mechanism to functionally translate actuation from the docking station to the microtweezer box (Fig. 1).

The packaged microtool consists of three main components: (1) a female luer hub, which allows for connection with the docking station and also houses the micro-drive mechanism, (2) an attached stainless steel hollow needle which provides both a physical structure in which to adhere the fixed body of the microtool, and a durable tract in which to allow translation of precise linear actuation of the drive system to the microtool, and (3) the internal micro-drive mechanism which consists of a spring-loaded button and a drive rod that runs through the needle cannula from the needle tip to the luer hub where it is seated into the button.

Because both fixed position and moving elements were required for relative motion, a tether-cable system was employed using the cannula of the stainless steel needle as the tether, and the drive rod as the cable. In addition to being an inexpensive, standardized docking component, the luer hub of the stainless steel needle houses the internal mechanism to allow translation of external linear actuation from the docking station to the microtweezer box. The MEMS microtweezer box and body are centered on the needle cannula axis, and the end of the microtweezer body is attached to a rectangular micro-milled notch in the outer face of the needle tip. The microtweezer box, which houses the body, is attached to the end of the drive rod. The spring loaded plastic button is held in place by a friction-locked rubber o-ring. This button is presented within the hub so that it can be contacted and linearly actuated by the output

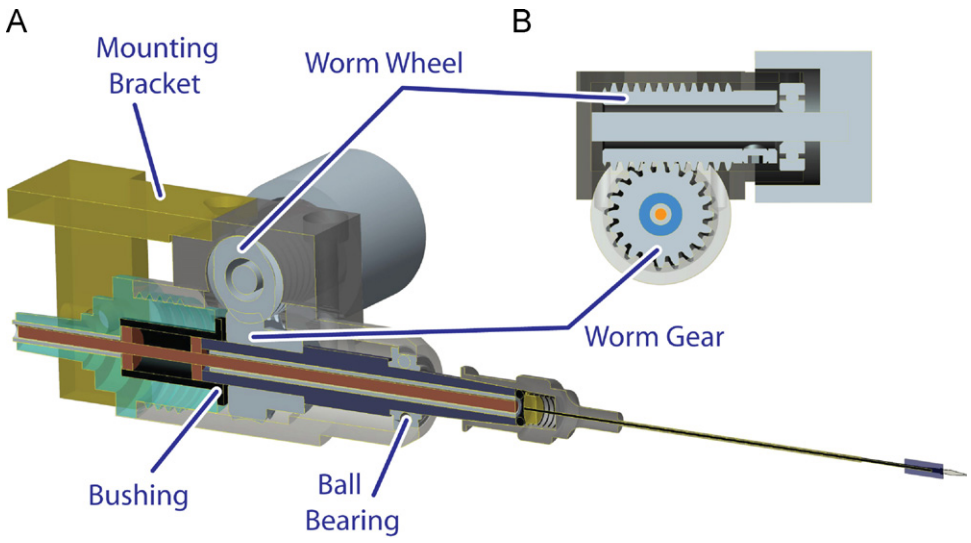

Fig. 3. (A) Cross-section of docking station schematic showing the rotationally isolated worm system that allows axial rotation of the packaged microtweezer. The worm gear and attached luer shaft (blue) can rotate independently with the housing (grey), as well as independently from the inner drive shaft (red), which will limit torsional loading on the spring loaded button of the luer-needle package. (B) Cross-section of the worm wheel and manually turn-able knob. (For interpretation of the references to color in the figure caption, the reader is referred to the web version of the article.)

shaft of the docking station. The motion of the drive rod relative to the needle shaft is translated to the tool box, which is then displaced relative to the tool body. Through this motion, the walls of the box channel make contact with the tool tips causing them to close.

This package design modality, which translates micron scale linear controller actuation into sub-micron scale resolution tip actuation, allows for easy, plug-n-play docking of tools. This package, which contains internally protected elements, and a stand-alone modular design, also reduces the complexity inherent in integrating sensors and various materials and geometries, as well as the physical integration into commercially available stages, micropositioners, and even SEM equipment.

2.4. Docking station and actuator

The docking station both physically and functionally connects the packaged microtweezer to a linear actuator, which opens and closes the tweezer tips using direct drive uni-axial motion. Due to modularity in the design, this docking station has

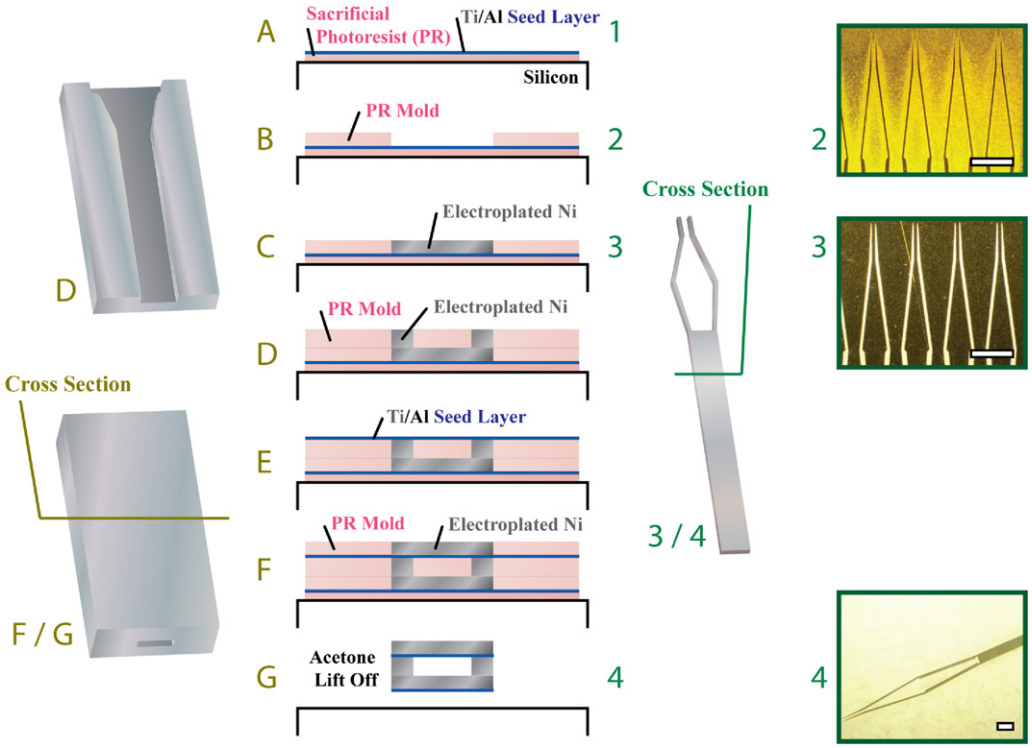

Fig. 4. Fabrication process flow for the three-layer microtweezer box (A–G) and the single layer microtweezer (1–4). Bright field photos are included that show the microtweezer construction at fabrication steps 2–4. All scale bars are 400 μm.

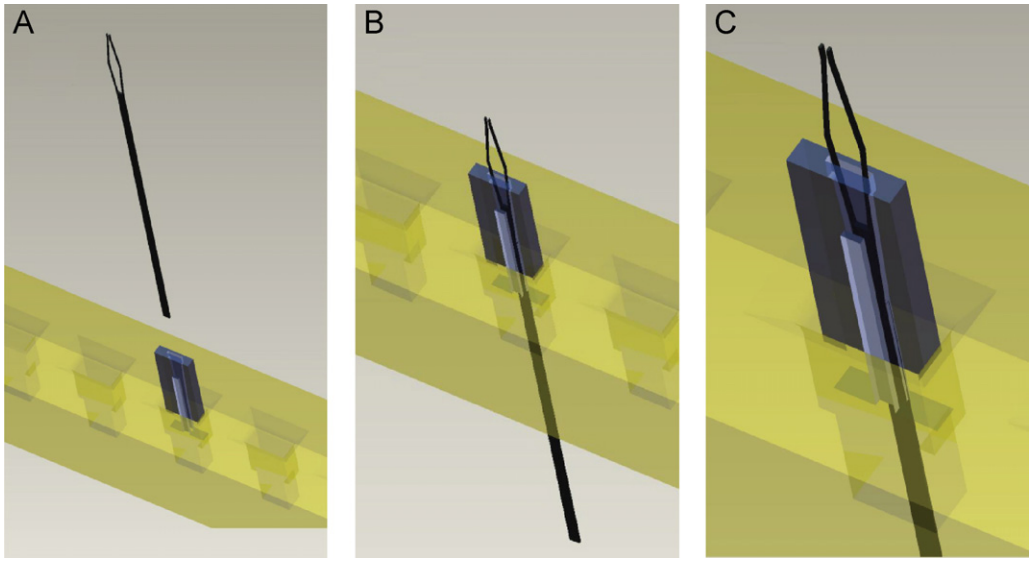

Fig. 5. Assembly process for attaching the assembled MEMS microtweezer microtool.

minimal manufacturing complexity. The industry standard luer docking interface provides plug and play functionality for loading and unloading of various microtools. The linear-actuation-based direct drive mechanism that runs through the luer fitting allows precise and controlled mechanical actuation of docked microtools.

Within the housing of the docking station is a torsionally isolated worm gear assembly with ball bearings which provides the ability to rotate the microtool about its axis (Fig. 3) in addition to the X, Y and Z motion provided by the stage. This rotational functionality allows for precise orientation of the microtool correctly for a variety of applications, and rotates independently from the internal drive rod's movement. The drive mechanism that travels throughout this docking system can be controlled by a manual or programmable actuator system connected to the rear of the docking station.

The housing for the docking station has a number of sockets for mounting brackets so that the docking station can be attached to any standard micropositioning or imaging stage.

The actuator reported in this work is composed of a manually turned micrometer head that is attached to a low-friction and flexible nitinol cable tether-cable system. Opening and closing of the microtweezer tips is thus achieved through the following steps: turning the micrometer, which creates relative linear motion that drives the nitinol tether-cable system; this system drives the spring-loaded drive rod internal to the docking station; this rod drives the spring loaded button of the microtweezer package, which advances the microtweezer box forward; which causes contact of the microtweezer channel with the tweezer beams, causing the tweezer tips at the end of the beams to close. Due to the modularity of the system, if rotational functionality was not required for a specific application, the docking station and nitinol system could be removed, and the actuator could be directed connected to the microtweezer package.

2.5. Stage

The stage allows for positional movement of the system in multiple linear and rotational axes and can be a commercially available robotic arm, micromanipulator, or micropositioner platform. Mounting of the docking station to a stage can be accomplished using a custom designed flat bracket.

3. Fabrication processes and device assembly

3.1. MEMS fabrication

Traditional photolithography and micromachining processes were used to fabricate the MEMS microtweezers. The tool body and the box were fabricated by electroplating a specified metal (nickel was used in this design, but copper, gold or rhodium microtweezers can also be developed using the same process) into a photolithographically defined mold on an electroplating seed layer (Fig. 4). A variety of substrate, mold and seed layer material combinations have been attempted for construction to provide the highest possible resolution of mold feature size, the most flexibility in mold geometries for thick single and multi-layer electroplating steps, convenience and success in microfabrication processing, and chemical resistance to the electroplating bath and lift-off processing steps. The optimized process solutions are described below.

Both the beam and box processes start with the spin coating of a thin (3–5 μm) sacrificial photoresist layer on a silicon wafer (Fig. 4A). This sacrificial layer will assist in lift off processing as well as electrically isolate the electroplating seed layer from the wafer, which prevents metal deposition on the edge and backside of the wafer during electroplating. The Ti/Al electroplating seed layer is then vapor deposited onto the sacrificial photoresist layer (Fig. 4A). The subsequent fabrication processes involve the creation of a series of photoresist molds in which a Ni is electroplated to form either the multiple layers of the box or the single layer of the tweezer (Fig. 4C–F). The box channel was created by patterning, and then dissolving a sacrificial photoresist structure in the second layer that ran the length of the box. A negative photoresist (NR-9-8000) was used to pattern the molds and sacrificial layers to (1) increase the temporal stability of the photoresist, (2) eliminate chemical reactivity that positive photoresist developers containing hydroxides and borates exhibit with an oxidation-sensitive aluminum electroplating seed layer [23], and (3) reduce chemical reactivity of photoresists while immersed in the electroplating bath. This negative resist was utilized to allow single-coat layers with thicknesses up to 30 μm. A power source supplied 100 mA of current to the electroplating seed layer on a 4 in. wafer resulting in a current density of 0.295 A/dm^2 and a plating rate of 2.3 μm/h. Following electroplating, a gentle acetone bath is used to remove the photoresist mold. For lift-off, the wafer is then placed in a fresh

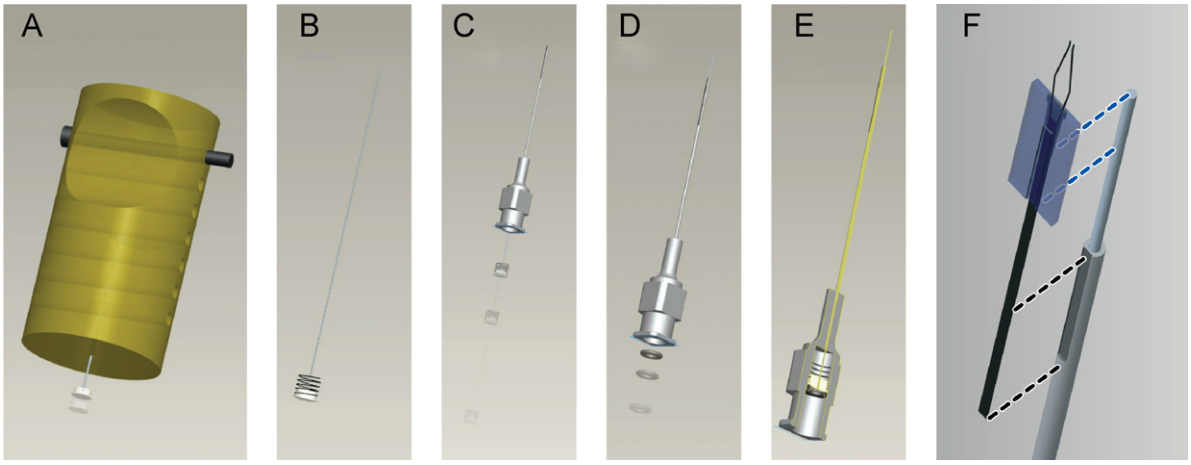

Fig. 6. Assembly process for the luer needle package and for attaching the assembled MEMS microtweezer microtool to the assembled package. The body of the microtweezer is placed in a notch at the end of the luer needle and glued, and the protruding end of the cable is glued to the notch on the underside of the box.

acetone bath with sonication to remove the sacrificial photoresist layer and ablate the thin film electroplating seed layer.

3.2. MEMS assembly

After the individual microtweezer body/tips and boxes were fabricated, they were assembled by inserting the end of the beam through the channel while imaged under an optical stereoscope, a clamped jig to hold the boxes, and hand-held forceps to manipulate and position the tweezer body to be inserted into the box.

Several jigs were constructed to facilitate device assembly in parallel (Fig. 5). The order of assembly was important due to nesting of the spring loaded button inside the housing of the luer needle and its physical connection with the MEMS components that are on the end of the luer needle. One end of the cable was inserted into a notch in the button and adhered with epoxy. A compression spring was inserted over the cable and nested over an outside groove in the button. The opposite end of the cable was then advanced into the luer housing and through the needle cannula until it comes out the end of the needle. An o-ring was then placed into the needle housing and seated by inserting a male luer fitting into the luer hub. This seated o-ring slightly compresses the spring, and creates a physical stop that controls the range of motion for the button.

The assembled MEMS device was then attached to the luer needle tool packaging by gluing the microtweezer body to the end of the needle, and the drive rod running through the needle cannula to the microtweezer box (Fig. 6). This simple interface between the package and MEMS device allows for reuse of the luer package system following detachment of the tweezer and box.

4. Mechanical modeling and evaluation

4.1. Microtweezer tip actuation modeling

Geometric modeling of the microtweezer tips allows for comparisons between theoretical predictions and experimental results, facilitating substantive modifications for subsequent design iterations. The microtweezer tips are composed of two beam structures with rectangular cross-sections. Because of the micro-scale dimensions of the device, and the same dimensional magnitude for both the width and thickness of the beam, the strength and mechanics of the tip motion can be modeled using beam theory [24–29]. The cross-sectional dimensions, material moduli, and predicted contact locations of the box channel wall and tweezer beams can be used to predict the geometries of the tweezer beams and tweezer tips throughout the actuation range of the box. Geometric equations were then solved to create an expected actuation of the

Table 1
Table of calculated values for modeling of tweezer beam actuation. This table shows the pertinent values in the model, and the equations used to determine the initial conditions and values during both drive and overdrive scenarios for actuation.

Calculated values	Initial value[a]	Actuation value
Shoulder angle: Φ	Φ_0	$\Phi = \tan^{-1}\left(\frac{B_1}{A_1}\right)$
Upper arm vertical vector: A_U	$A_{U0} = C_U \cdot \cos(\Phi_0)$	$A_{U0} = C_U \cdot \cos(\Phi_0)$
Upper arm horizontal vector: B_U	$B_{U0} = C_U \cdot \sin(\Phi_0)$	$B_{U0} = C_U \cdot \sin(\Phi_0)$
Elbow angle – upper arm: Θ_U	$\Theta_{U0} = 90 - \Phi_0$	$\Theta_U = 90 - \Phi$
Elbow angle – forearm: Θ_F	$\Theta_{F0} = \Theta_{TOT} - \Theta_{U0}$	$\Theta_{F0} = \Theta_{TOT} - (90 - \Theta)$
Forearm vertical vector: A_F	$A_{F0} = C_F \cdot \sin(\Phi_{F0})$	
Forearm horizontal vector: B_F	$B_{F0} = C_F \cdot \cos(\Phi_{F0})$	$B_F = C_F \cdot \cos(\Phi_F)$
Elbow separation: W		$W = (B_U + T_{BODY}) \cdot 2$
Moment vertical vector: A_1	$A_{10} = \frac{B_{10}}{\tan(\Phi_0)}$	$A_1 = A_{10} - Actuation$
Moment length: C_1	$C_{10} = \frac{B_{10}}{\sin(\Phi_0)}$	$C_1 = \frac{B_1}{\sin(\Phi)}$
Moment horizontal vector: B_1	$B_{10} = \frac{N + T_{BODY}}{2}$	$B_{1,\,Drive} = \frac{N + T_{BODY}}{2}$
		$B_{1,\,Overdrive} = B_{10} - (A_t - A_{U,\,Trans}) \cdot \tan(\Omega)$
[b]Actuation transition: $A_{U,\,Trans}$	$A_{U,\,Trans} = \frac{B_{10}}{\tan(\sin^{-1}(B_{10}/C_U))}$	
Tip separation: T_s		$T_s = (B_U - B_F - T_{BEAM}) \cdot 2 + T_{BODY}$

[a] Assumes tweezer beams and channel notch at initial contact point.
[b] When action turns from drive to overdrive.

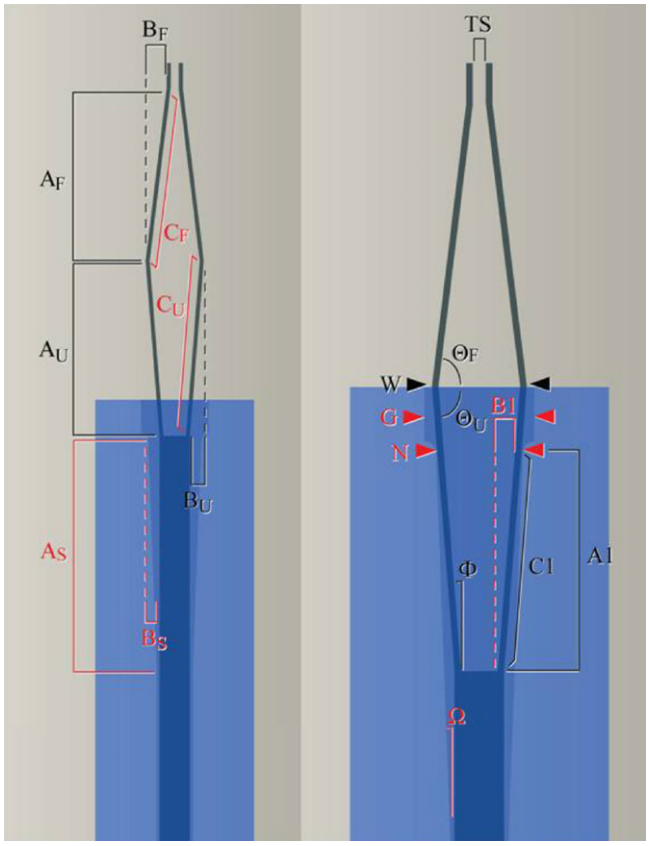

Fig. 7. Schematic of the tweezer body and beams housed within the channel, and the pertinent geometric dimensions that are considered when calculating the predicted actuation behavior. Static dimensions are highlighted in red, and dynamic dimensions, which change value over the course of actuation, are in black. (For interpretation of the references to color in the figure caption, the reader is referred to the web version of the article.)

tweezer beams based on the beam geometries, the box channel geometries, and the box location relative to the tweezer body and beams.

Tweezer and box geometries (Table 1, Fig. 7) could then be designed to provide nearly linear closing of the tips through both regular and overdrive actuation. The separation of the tips is shown based on the actuation distance of the box (Fig. 8). For a tweezer with a tip separation of 330 μm, a box actuation of 1.09 mm is required to close the tips, and this mechanical advantage of roughly 1:3 can allow increased actuation resolution.

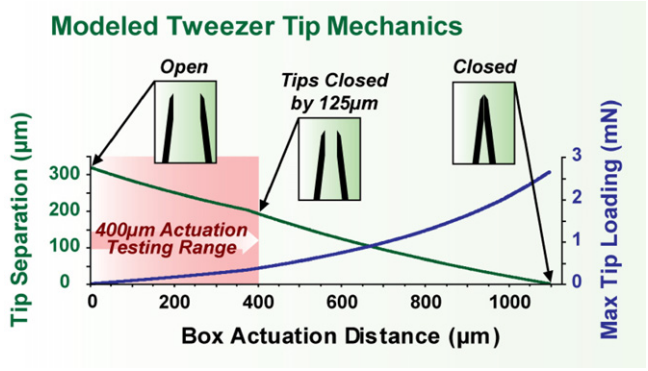

Fig. 8. Modeling data for separation of tips based on actuation distance of box, and maximal force loading seen at the inner face of the tweezer.

4.2. Microtweezer tip force modeling

The bending and deflection forces of the tweezer beams can be predicted based on the expected moment-force arm that exists on the shoulder of the tweezer. Constituent horizontal and vertical (or normal and tangential) force vectors can be created from the linear force vector which is in turn a result of the advancement of the box on the tweezer beam (Figs. 7 and 9). These force vectors can be used to predict the pushing force for box advancement that will be required to deflect the tweezer beams, as well as different moments created along the tweezer beam, and most importantly, the forces seen at the tips of the tweezers as they close. Because of the predictable bending behavior, Castigliano's second theorem of beam deflection can be used to calculate the forces required to cause specified deflections of the tweezer beams [30–32]. This modeling method considers the cross-sectional geometries of the beam, the beam material and modulus, the moment of inertia, and moment arm of force loading. Cantilever deflection models were less relatable as the thickness of the beam on the axis of deflection is neither 'thin' in micro-structure considerations, and is not considerably smaller in dimension than the width, or the normal cross-sectional dimension. Castigliano's theorem can be rearranged as (1) and (2) to calculate force (F) as a function of single-axis deflection (δ) and strain energy (U):

$$F_i = \frac{\partial U}{\partial \delta_i} \tag{1}$$

$$\delta = \frac{\partial U}{\partial F} \tag{2}$$

$$\delta = \frac{\partial}{\partial F}\int_0^L \frac{M^2}{2 \cdot E \cdot I} dl \tag{3}$$

$$\delta = \int_0^L \frac{F \cdot l^2}{E \cdot I} dl \tag{4}$$

$$\delta = \frac{F \cdot L^3}{3 \cdot E \cdot I} \tag{5}$$

$$F = \frac{3 \cdot \delta \cdot E \cdot I}{L^3} \tag{6}$$

Strain energy (U) was calculated as (3) from the known quantities of the point of bend to moment length (l), elastic modulus (E), and inertia (I). After moving the force load into the integral (4), and

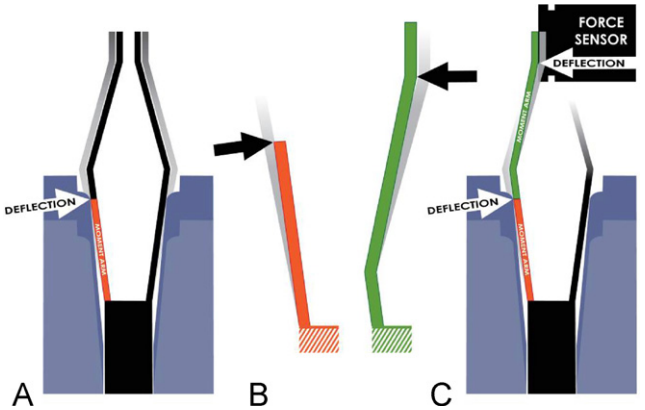

Fig. 9. Cartoon demonstrating the geometric modeling used to predict forces seen at the tip. This tip force calculation, along with calculation of frictional and loading forces seen on the tweezer beams and in the mechanical packaging aid in the geometric and packaging design process and enhance understanding of performance. (A) Normal tweezer deflection performance, and (B and C) the double moment arm on the tweezer beam caused by movement isolation from loading on the force sensor.

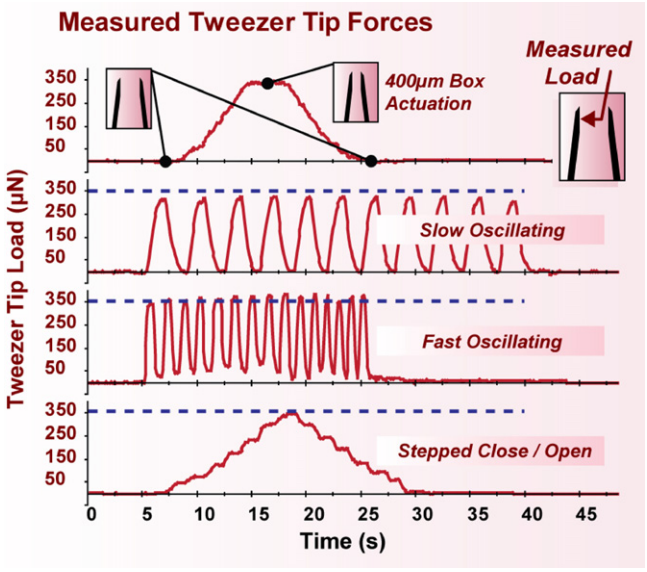

Fig. 10. Measured force on inner face of closing tweezer tip. Average maximal forces from 125 μm tip deflections were 0.321 mN, 0.367 mN, 0.339 mN, and 0.335 mN for oscillating, fast oscillating, slow close/open, and stepped close/open actuations respectively. The dashed blue line denotes the maximal force calculated for a 125 μm closing. (For interpretation of the references to color in the figure caption, the reader is referred to the web version of the article.)

integrating with respect to the moment length (5), the equation can be re-arranged to determine force.

A conservative application of these equations that used static calculations of moment arm length and values of deflection predicted from the geometric modeling, provided maximal forces for tweezer beam deflection throughout the actuation cycle. Applied to a double moment-arm model of tweezer actuation (Fig. 9), maximal forces of roughly 358 μN are expected to be seen at the inner face of the tweezer tip during a closing regimen of 125 μm.

4.3. Microtweezer tip force characterization

Following assembly of the packaged MEMS devices, docking station, and actuator, the forces exerted by the inner faces of the tweezer tips were measured under a variety of actuation schemes using the MTS NanoUTM system (Oak Ridge, TN) (Fig. 10). Quickly oscillating tip deflections of 125 μm (oscillating period for 250 μm open-close movement averaged less than 1.5 s) delivered via the manual actuator showed average maximal forces of 367 μN with a standard deviation of 1.1 μN, which compares well with the modeled force in the previous section. The maximal static forces calculated from the double-moment arm model compare well with these measured forces (Fig. 11).

These measured forces suggests a beam spring constant of 2.936 N/m for this actuation regimen. While this small spring constant enables manipulation of delicate microstructures like biological constructs, the tip force is strong enough to overcome the adhesion of cells to substrates [33] and to lift solid structures over 10 mg. With over-actuation, which would cause increased inner-tip face forces and noticeable beam deflection, far heavier objects could be lifted by our microtweezers.

4.4. Microtweezer box actuation force modeling

Data from both measured tweezer tips forces and mechanical modeling were used to predict static and kinetic frictional loading (Fig. 10) at the tweezer beam–box channel interface. Point contacts were assumed for both drive (rounded drive contact, linear tweezer beam) and over-drive conditions (flat over-drive contact

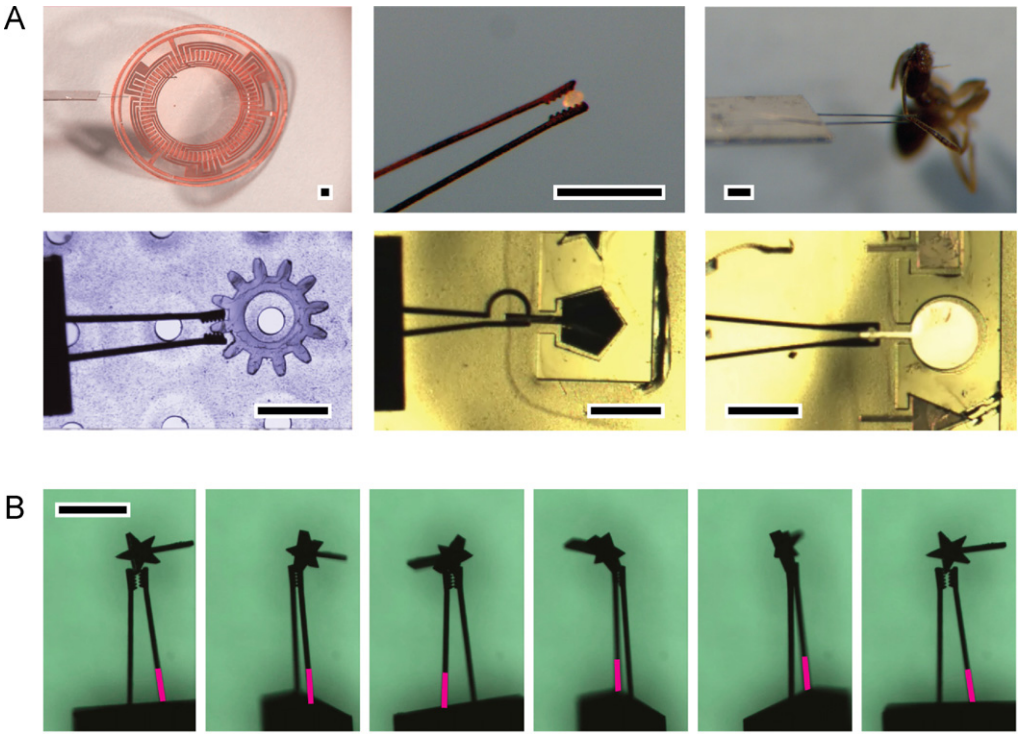

Fig. 11. (A) Stereoscopic and microscopic photographs demonstrating the wide range of applications for microtweezers with varying tip styles. Microtweezers are shown positioning MEMS devices and material samples as well as interfacing with biological samples. (B) The continuous rotational functionality of the microtweezer about its axis is demonstrated in a series of photographs. The same tweezer beam is labeled in pink in each photo to assist in visualizing the rotation. All microtweezers shown here have thickness of 25 μm, and beam widths of 40 μm, and all scale bars are 500 μm. (For interpretation of the references to color in the figure caption, the reader is referred to the web version of the article.)

wall, pointed tweezer beam elbow). Over 400 μm of box actuation resulting in 125 μm of tweezer tip closing, with a calculated first moment arm loading of 341 μN on the upper arm of tweezer beam, and a shoulder angle of 3.45°, maximal frictional forces of 4.832 mN are expected normal to tweezer beam deflection angle. The calculated tweezer beam moment and frictional loading for this 400 μm actuation suggests a minimal forward force of 4.835 mN is required to advance the box. Because the tweezer beam moment arm length changes over the course of actuation, a linear spring constant is difficult to calculate due to the cubic relationship between moment length and force. A semi-linear spring constant region over the 400 μm box actuation suggests a spring constant of 12.09 mN/mm exists on the first moment arm.

For the MEMS luer-needle packaging, these calculated forces were used to determine the minimal spring rate (k) required of the spring-loaded button to overcome slip-stick across the tweezer beam–box channel interface. A spring with a constant of 21.0 mN/mm was selected for the luer packaging.

5. Manipulation of microstructures and samples

Attaching the microtweezer system to a Signatone (Lucas Signatone, Gilroy, CA) micromanipulator with an additional control knob for tweezer actuation (Fig. 11) has allowed for use in a variety of manipulation and positioning applications. Coupled with this probing station, the microtweezer system has the ability to manipulate image markers, crystals, and other small structures, as well as large devices such as MEMS stators and microgears. This positioning system has also been used to precisely direct the microtool's location and use within cell cultures, and to micromanipulate a variety of devices and biological samples (Fig. 7). Due to the spring-loaded direct drive mechanism of the MEMS packaging, the microtweezer device performance is not significantly affected while immersed in aqueous solutions which is a significant advantage over current solutions in micromanipulation.

6. Conclusion

A fully packaged mechanically actuated microtweezer system is presented in this paper. This system relies on a mechanical microcam mechanism to actuate the microtool tips. The microtweezers and the sleeve they sit in are both fabricated using standard electroplating processes providing potential for multitude of materials. In addition to providing enhanced functionality and ease of attachment to micromanipulators and micropositioners, this system has multiple advantages over previously developed systems including simplified design, durability, flexibility, and modularity. Due to its elegant device design, this system provides a platform in which to integrate additional functionality and sensors that can enhance its application space.

No change in tweezer performance was observed following several micromanipulation operations, and future cycle testing could be utilized to verify device consistency and longevity. Given the material composition and mechanics, the longevity of the nickel tool is generally expected to be comparable with silicon based alternatives [29]. Metals have higher flaw tolerance than ceramics, and will not mechanically or functionally fail when the yield strength is surpassed from localized stresses and strains that result from complex and unpredictable loading conditions [30].

Characterization of the system shows that mechanical modeling can be used successfully to predict tweezer performance. This modeling can aid in tailoring the tweezer geometries and dimensions for specific applications, and the material and mechanical properties of the MEMS packaging components. Prescribed, repeatable actuations and forces can be induced with the microtool tips even with the use of a manual controller, and the mechanical actuation mechanism allows for introduction into aqueous and biological environments. This can allow this system, for example, to be used to induce prescribed biaxial compression loading onto cells in tissue or to microposition electrically and thermally sensitive components during micro-assembly procedures [34]. Overall, this system's performance and ease of use can provide the means to create and enhance a multitude of experimental preparations in the material, semiconductor, and biomedical engineering fields.

Acknowledgments

The authors wish to thank Scott Bair and Jevin Scrivens Ph.D. for their support with packaging and mechanical design of the docking station and actuator, and Yoonsu Choi Ph.D. for original microtweezer design.

References

[1] A. Manz, N. Graber, H.M. Widmer, Miniaturized total chemical-analysis systems—a novel concept for chemical sensing, Sensors and Actuators B Chemical 1 (January) (1990) 244–248.
[2] A. Stett, U. Egert, E. Guenther, F. Hofmann, T. Meyer, W. Nisch, H. Haemmerle, Biological application of microelectrode arrays in drug discovery and basic research, Analytical and Bioanalytical Chemistry 377 (October) (2003) 486–495.
[3] K.D. Wise, Silicon microsystems for neuroscience and neural prostheses, IEEE Engineering in Medicine and Biology Magazine 24 (September–October) (2005) 22–29.
[4] T. Velten, H.H. Ruf, D. Barrow, N. Aspragathos, P. Lazarou, E. Jung, C.K. Malek, M. Richter, J. Kruckow, Packaging of bio-MEMS: strategies, technologies, and applications, IEEE Transactions on Advanced Packaging 28 (November) (2005) 533–546.
[5] R.R. Tummala, Fundamentals of Microsystems Packaging, McGraw-Hill, 2001.
[6] Y. Choi, J. Ross, B. Wester, M.G. Allen, Mechanically driven microtweezers with integrated microelectrodes, Journal of Micromechanics and Microengineering 18 (June) (2008).
[7] B.A. Wester, J.D. Ross, S. Rajaraman, M.G. Allen, Packaging and characterization of mechanically actuated microtweezers for biomedical applications, in: IEEE EMBC Minneapolis, MN, 2009.
[8] F. Beyeler, A. Neild, S. Oberti, D.J. Bell, Y. Sun, J. Dual, B.J. Nelson, Monolithically fabricated microgripper with integrated force sensor for manipulating microobjects and biological cells aligned in an ultrasonic field, Journal of Microelectromechanical Systems 16 (February) (2007) 7–15.
[9] P. Boggild, T.M. Hansen, C. Tanasa, F. Grey, Fabrication and actuation of customized nanotweezers with a 25 nm gap, Proceedings, 8th Foresight Conference on Molecular Nanotechnology, 2001, pp. 331–335.
[10] N. Chronis, L.P. Lee, Electrothermally activated SU-8 microgripper for single cell manipulation in solution, Journal of Microelectromechanical Systems 14 (August) (2005) 857–863.
[11] M.B. Cohn, K.F. Bohringer, J.M. Noworolski, A. Singh, C.G. Keller, K.Y. Goldberg, R.T. Howe, Microassembly technologies for MEMS, in: Materials and Device Characterization in Micromachining, Santa Clara, CA, 1998, pp. 2–16.
[12] N. Dechev, W.L. Cleghorn, J.K. Mills, Microassembly of 3-D microstructures using a compliant, passive microgripper, Journal of Microelectromechanical Systems 13 (April) (2004) 176–189.
[13] C. Haber, D. Wirtz, Magnetic tweezers for DNA micromanipulation, Review of Scientific Instruments 71 (2000) 4561–4570.
[14] S.K. Jericho, M.H. Jericho, T. Hubbard, M. Kujath, Micro-electro-mechanical systems microtweezers for the manipulation of bacteria and small particles, Review of Scientific Instruments 75 (May) (2004) 1280–1282.
[15] C.G. Keller, R.T. Howe, Hexsil tweezers for teleoperated micro-assembly, in: Micro Electro Mechanical Systems, 1997, MEMS '97, Proceedings, IEEE, Tenth Annual International Workshop, 1997, pp. 72–77.
[16] W. Nogimori, K. Irisa, M. Ando, Y. Naruse, A laser-powered micro-gripper, in: Micro Electro Mechanical Systems, 1997, MEMS '97, Proceedings, IEEE, Tenth Annual International Workshop, 1997, pp. 267–271.
[17] R. Tharmann, M. Keller, J. Uhde, A. Bausch, Active networks studied by magnetic tweezers microrheometry and torsional macrorheometry, Proceedings, 47th Annual Meeting of the Biophysical-Society, 2003, pp. 247A.
[18] G.T.A. Kovacs, Micromachined Transducers: Sourcebook, McGraw-Hill, 1998.
[19] Y. Choi, M.G. Allen, J.D. Ross, S.P. DeWeerth, Microfabricated Mechanically Actuated Microtool and Methods, vol. 7461882, USPTO, USA, 2005.
[20] G.E. Yang, J.A. Gaines, B.J. Nelson, A supervisory wafer-level 3D microassembly system for hybrid MEMS fabrication, Journal of Intelligent & Robotic Systems 37 (May) (2003) 43–68.
[21] U. Srinivasan, M.R. Houston, R.T. Howe, R. Maboudian, Alkyltrichlorosilane-based self-assembled monolayer films for stiction reduction in silicon micromachines, Journal of Microelectromechanical Systems 7 (June) (1998) 252–260.
[22] Cambridge Nanotechnologies, 2009.

[23] P.E. Bakeman, H.K. Lee, S.E. Luce, Protection of Aluminum Metallization Against Chemical Attack During Photoresist Development, vol. 5480748, USA, 1996.
[24] M. Dafflon, B. Lorent, R. Clavel, F. Beyeler, B.J. Nelson, Characterization of micro manipulation tasks oriented with various controlled conditions by microtweezers, International Workshop on MIcroFactories (2006).
[25] J. Fraser, T. Hubbard, M. Kujath, Theoretical and experimental analysis of an off-chip microgripper, Canadian Journal of Electrical and Computer Engineering-Revue Canadienne De Genie Electrique Et Informatique 31 (Spring) (2006) 77–84.
[26] J.M. Gere, Mechanics of Materials, vol. 5: Brooks-Cole, 2000.
[27] I.P.F. Harouche, C. Shafai, R.G. Gordon, Design and simulation of microtweezers using a controlled displacement comb drive, in: Canadian Conference on Electrical and Computer Engineering, 2006, pp. 341–343.
[28] D.H. Kim, M.G. Lee, B. Kim, Y. Sun, A superelastic alloy microgripper with embedded electromagnetic actuators and piezoelectric force sensors: a numerical and experimental study, Smart Materials & Structures 14 (December) (2005) 1265–1272.
[29] K.P. Larsen, A.A. Rasmussen, J.T. Ravnkilde, M. Ginnerup, O. Hansen, MEMS device for bending test: measurements of fatigue and creep of electroplated nickel, in: Micro Electro Mechanical Systems, 2002. MEMS '02, Proceedings, IEEE, Fifteenth Annual International Workshop, Las Vegas, Nevada, 2002, pp. 156–164.
[30] J.M. Gere, B.J. Goodno, Mechanics of Materials, 7th ed., CI Engineering, 2009.
[31] L.S. Li, X.D. Meng, L. HX, Analysis and stress optimization design of an S-shaped micro spring, in: Manufacturing Science and Engineering, Zhuhai, China, 2009, pp. 2500–2504.
[32] Y.B. Wu, G.F. Ding, C.C. Zhang, J.A. Wang, S.P. Mao, H. Wang, Design and implementation of a bistable microcantilever actuator for magnetostatic latching relay, Microelectronics Journal 41 (June) (2010) 325–330.
[33] P. Tsang, G. Li, Y. Brun, L.B. Freund, J. Tang, Adhesion of single bacterial cells in the micronewton range, in: Proceedings of the National Academy of Sciences of the USA, vol. 103, 2006, pp. 5764–5768.
[34] B.A. Wester, J.D. Ross, S. Rajaraman, M. Kuykendal, G. Guvanasen, M.G. Allen, M.C. LaPlaca, A single-unit neural injury model using mechanically actuated microtweezers, Society for Neuroscience (2009).

Biographies

Brock A. Wester was born in Okinawa, Japan, in 1981. He received the B.S. degree in computer engineering from the Georgia Institute of Technology, Atlanta, GA, in 2004, and has defended his Ph.D. thesis in biomedical engineering from Georgia Institute of Technology and Emory University, Atlanta, GA, in 2010. He joined Matsushita Mobile Communications Division in 2000 as a computer engineering cooperative student employee. In 2009, he co-founded NanoGrip Technologies, Inc. and held the position of Chief Technology Officer and Board Member. His research areas include microfabrication, MEMS, packaging, prototyping, machining, software engineering, and biomedical engineering. Mr. Wester is a member of the Institute of Electrical and Electronics Engineers (IEEE), Society for Neuroscience (SFN) and the National Neurotrauma Society (NNS).

Swaminathan Rajaraman was born in New Delhi, India in 1977. He received a B.S. degree in electronics engineering from Bharathidasan University (Trichy, India) in 1998, a M.S. degree in electrical engineering from the University of Cincinnati (Cincinnati, OH) in 2001 and a Ph.D. degree in electrical engineering from the Georgia Institute of Technology (Atlanta, GA) in 2009. He has worked as a process development engineer at Analog Devices Inc. (Cambridge, MA) from 2001 to 2002 and as a MEMS Engineer at CardioMEMS Inc. (Atlanta, GA) from 2004 to 2005. He has also co-founded two start-up companies both based in Atlanta, GA – Axion BioSystems Inc., in 2008 and NanoGrip Technologies Inc. in 2009. He is currently the Director of MEMS R&D and manufacturing at Axion BioSystems Inc. His research interests include micro/nanofabrication, neuralMEMS, micro/nanotools, microTAS, microneedles, pressure sensors, nanosensors and microelectronic and biomedical devices packaging. He is a member of the Electrochemical Society and recently served as a track chair for bioelectric sensors at IEEE EMBC 2010. He also participates frequently in National Nanotechnology Infrastructure Network (NNIN) programs to promote micro/nanotechnology in the US.